ELSEVIER

Behavioural Brain Research 135 (2002) 167–178

BEHAVIOURAL BRAIN RESEARCH

www.elsevier.com/locate/bbr

Research report

Receptive field structure in cortical area 3b of the alert monkey

James J. DiCarlo [a], Kenneth O. Johnson [b,*]

[a] *McGovern Institute for Brain Research/Department of Brain and Cognitive Sciences, M.I.T., Cambridge, MA, USA*
[b] *Krieger Mind/Brain Institute and Department of Neuroscience, Johns Hopkins University, Baltimore, MD, USA*

Received in revised form 9 April 2002; accepted 1 May 2002

Abstract

More than 350 neurons with fingerpad receptive fields (RFs) were studied in cortical area 3b of three alert monkeys. Random dot patterns, which contain all stimulus patterns with equal probability, were scanned across these RFs at three velocities and eight directions to reveal the RFs' spatial and temporal structure. Area 3b RFs are characterized by three components: (1) a single, central excitatory region of short duration, (2) one or more inhibitory regions, also of short duration, that are adjacent to and nearly synchronous with the excitation, and (3) a region of inhibition that overlaps the excitation partially or totally and is temporally delayed with respect to the first two components. As a result of these properties, RF spatial structure depends on scanning direction but is virtually unaffected by changes in scanning velocity. This RF characterization, which is derived solely from responses to scanned random-dot patterns, predicts a neuron's responses to random patterns accurately, as expected, but it also predicts orientation sensitivity and preferred orientation measured with a scanned bar. Both orientation sensitivity and the ratio of coincident inhibition (number 2 above) to excitation are stronger in the supra- and infragranular layers than in layer IV.

Keywords: Neurophysiology; Somatosensory; Cortex; Receptive field; Reverse correlation; Orientation sensitivity; Directional sensitivity

1. Introduction

In this paper, we describe the results of three studies aimed at determining the spatial and temporal structure of excitation and inhibition that constitute the receptive fields (RFs) in the glabrous skin region of area 3b of the alert monkey [6–8]. Previous studies of the response properties of neurons in area 3b have reported excitatory summation [11], surround inhibition [15,25], directional selectivity [13,34,36], orientation selectivity [13,29,34], and selectivity for the features of complex, scanned patterns [2,18,27] but none has elucidated the RF structure that underlies these responses.

The primary stimulus patterns were arrays of raised dots, 400 μm high, distributed randomly within a rectangular region 28 mm wide and 175 or 250 mm long [6]. Random-dot patterns are unbiased in the sense that all possible patterns with the specified dot density (10 dots mm^{-2} in this case) are equally likely and the probability of a repeated pattern is virtually zero. A subset of neurons was also studied with scanned, oriented bars. The stimulus patterns were wrapped around and glued to a cylindrical drum, 320 mm in circumference, which was mounted on a rotating drum stimulator and applied to the skin [17].

The random dot patterns were applied to the skin containing the RF for 10–14 min to obtain the impulse response data used to infer the RF structure. During that period approximately 20 000 different stimuli were presented. As a result, all regions of excitation and inhibition in each RF were probed singly and in combination. We assumed that each small region of skin had a positive, negative or zero effect on the firing rate when stimulated and that the instantaneous firing rate was equal to the sum of these effects. Specifically, we subdivided a 10×10 mm square region of skin containing the RF into a grid of 625 (25×25) subregions, each 0.4×0.4 mm square. We then determined the contribution of each subregion to the observed neural response with multiple regression. The grid of 625 positive (excitatory) and negative (inhibitory) values are

* Corresponding author. Tel.: +1-410-516-6412; fax: +1-410-516-8648
E-mail address: kenneth.johnson@jhu.edu (K.O. Johnson).

0166-4328/02/$ - see front matter
PII: S0166-4328(02)00162-6

the weights that produce the best (least-squared error) approximation of the observed firing rates when convolved with the stimulus pattern. The units of these weights are impulses per second per mm indentation (imp s^{-1} mm^{-1}). The integral of the excitatory (inhibitory) weights is referred to as the excitatory (inhibitory) mass of the RF [6]. The relationship of this RF estimation method to other methods (e.g. reverse correlation) is discussed in DiCarlo and Johnson [7].

Every neuron with a well isolated action potential and a RF on the distal pad of one of the digits (2–5) was studied. The only exceptions were neurons with RFs on the sides of the pads that could not be positioned under the drum stimulator. Each of the three monkeys performed a visual detection task unrelated to the stimulus.

A typical area 3b RF is shown in Fig. 1. Each RF weight value can be interpreted as the instantaneous change in firing rate that occurs when its 400 × 400 μm skin region is depressed by a stimulus feature 400 μm high (the dot relief) moving from proximal to distal at 40 mm s^{-1}. The RF map in Fig. 1A shows that this neuron had a region of intense excitation followed by a slightly larger region of inhibition and that both regions were oriented at about 45° relative to the proximal–distal axis of the finger. The relationship between the weight pattern and the responses can be seen by inspecting Fig. 1B–D. Whenever one or more dots occurred anywhere within the darkened region of the RF the probability of firing increased. When dots occurred only within the white, inhibitory region there was no effect on firing rate because this neuron, like most neurons in the study, had no background discharge to be inhibited. However, whenever one or more dots occurred in the inhibitory region at the same time as dots in the excitatory region the probability of firing was reduced relative to that expected from stimulation of the excitatory region alone. Three instances are shown in Fig. 1B–D. The left-most example shows an instant in the ongoing interaction between the RF and the stimulus pattern where three dots happen to lie within the excitatory region of the RF. This alignment predicts an intense response, which is displayed at the tip of the arrowhead in Fig. 1C. The actual response is displayed at the comparable location in Fig. 1D. The second example illustrates an alignment where only a single dot lies within the excitatory region. The predicted (1C) and actual (1D) responses are much less intense than in the first example. The third example shows an alignment with a stimulus dot at exactly the same place within the excitatory subfield but also with two dots within the inhibitory field. The predicted (1C) and actual (1D) result is a cessation of firing. Fig. 1E shows a continuous trace of the predicted and observed firing rates across the single scan indicated by the arrows to the left and right of Fig. 1C and D.

In the first study, we studied over 300 area 3b RFs using random dots scanned from distal to proximal at a single scanning velocity (40 mm s^{-1}). In the second and third studies, we examined the effect of changes in scanning velocity (20, 40 and 80 mm s^{-1}) and changes in scanning direction on some of these RFs. Considering the results of all three studies, we reached the following conclusion. Ninety-five percent of area 3b neurons RFs can be described by three components: (1) a single, central excitatory region of short duration, (2) one or more inhibitory regions that are adjacent to and nearly synchronous with the excitation, and (3) an inhibitory region that overlaps the excitation partially or totally and is delayed with respect to the first two components. The remaining 5% had two or more regions of excitation. No attempt was made to analyze those RFs in more detail. We refer to the first inhibitory component as the fixed inhibition because its location and size were independent of scanning velocity and direction; we refer to the second inhibitory component as the lagged inhibition. The results that led to this conclusion are outlined below.

2. Study 1: Random dots scanned distally at 40 mm s^{-1}

Two hundred and forty-seven of the 330 neurons studied with random dot patterns scanned distally over the distal pad responded with enough action potentials to yield highly repeatable RF estimates that were suitable for further analysis [6]. The excitatory region was circular or ovoid and it varied greatly in area and intensity. The excitatory areas varied more than 10 to 1 (3–43 mm^2; mean, 14 mm^2). The excitatory strength—the integral of excitation over the excitatory area, which we refer to as excitatory mass—varied by 50 to 1 (210–10 300 mass units; mean 2140).

The inhibitory regions occurred on one side (54%), opposite sides (15%), two adjacent sides (9%), three sides (14%), or on all four sides (3%) of the excitatory center. In the remaining cases (5%) there was more than one significant region of excitation with interdigitated inhibition. The inhibitory area was, on average, about 30% larger than the excitatory area (18 versus 14 mm^2 means) and, like the excitatory area, varied greatly (from 1 to 47 mm^2). The inhibitory mass, like the excitatory mass, varied by 50 to 1 (125–6830 mass units; mean 1620 mass units). There was no evidence of clustering into distinct RF types. The distributions of excitatory and inhibitory areas and masses were all lognormal; the excitatory and inhibitory masses were more closely correlated ($\rho = 0.56$) than were the areas ($\Delta = 0.26$).

The excitatory regions were on average almost twice as long as they were wide (mean aspect ratio, 1.7); the individual aspect ratios ranged from 1 (circular) to 3.6

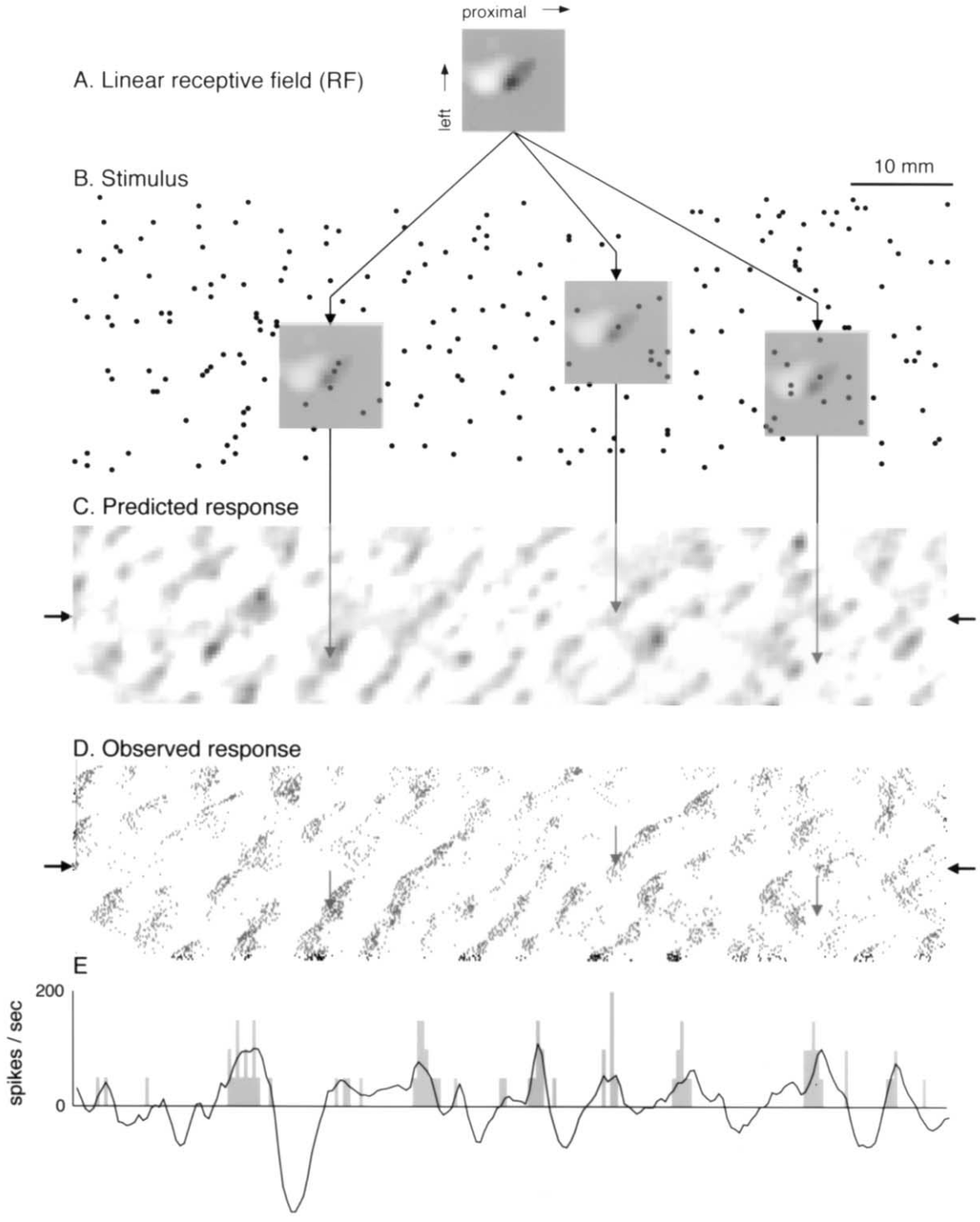

Fig. 1

(highly elongated). The orientations of the long axes of the excitatory regions were distributed uniformly in all directions relative to the axis of the finger. In those cases in which the inhibition could reasonably be assigned an aspect ratio and orientation (80% of the inhibitory mass occurred in a single, continuous lobe in 182 RFs) the inhibition was, on average, more elongated than the excitation and in the majority of the cases (65%) was aligned to within 20° of the excitation.

A striking feature of these data was the distal bias in the location of the inhibition relative to the excitation. When the overall center of mass of the inhibition was calculated, it was found to be distal to the center of excitation in 86% (212/247) of RFs; in 20% (49/247) of

the RFs, the center of inhibition was 3 mm or more distal to the center of excitation. There are two possible explanations for this bias. One is that there is, in fact, a distal bias in the location of inhibition relative to excitation. The other is that inhibition is delayed with respect to the excitation and therefore appears to be displaced from the excitation in the scanning direction (proximal-to-distal). This can be explained as follows: Suppose the centers of excitation and inhibition coincide, but inhibition is delayed by 75 ms relative to the excitation. A stimulus dot moving through the neuron's RF will produce an excitatory effect and then, 75 ms later, an inhibitory effect. However, by that time the dot will have moved past the RF center by 3 mm (at 40 mm s^{-1}). The inhibition will appear to have arisen from a region displaced 3 mm distal to the excitation. A third possibility, which emerges as the answer in the third study, is that the inhibition overlaps the excitation and is delayed much less (e.g. 20–30 ms), which produces a distal shift in the inhibition by only about 1 mm. This is revealed as net inhibition only at the distal edge of the excitation, whose radius ranges from 1 to 4 mm. These possibilities cannot be distinguished when scanning the random dot stimulus in a single direction at a single velocity. Note, however, that they can be distinguished by varying the scanning direction or scanning velocity. If the inhibition is delayed it will always appear to be trail behind the excitation in the scanning direction. If the 3 mm distal bias in inhibition at 40 mm s^{-1} is accounted for by a 75 ms delay then that bias will increase to 6 mm at 80 mm s^{-1}.

The results of varying velocity and direction are not as simple as might be expected. The RF geometry is virtually unaffected by changes in scanning velocity (study 2), which suggests that inhibition is not delayed relative to excitation. However, when scanning direction is varied (study 3) a significant fraction of the inhibition is shown to lag behind the excitation by an average of 30 ms. The seeming contradiction is resolved by showing how overlapping excitation and inhibition function to produce velocity invariance even when there is substantial delay between the two.

3. Study 2: random dots scanned distally at 20, 40, and 80 mm s^{-1}

The RF of every neuron is defined in space and time (see Ref. [7], Appendix A). Because we do not initially know the delay between the stimulus and the excitatory and inhibitory effects, our RF estimation procedure assigns each response component to the stimulus location at the time the response occurred. For this reason, the estimated location of each RF component is displaced in the scanning direction from its true location by a distance proportional to the delay and the scanning velocity. A differential delay between two components results in differential displacement in the scanning direction that is proportional to the scanning velocity and the differential delay. Similarly, excitatory or inhibitory persistence produces effects that are smeared in the scanning direction over a distance proportional to the persistence and the scanning velocity. Thus, relative delay between excitation and inhibition appears as a growth in separation between the two as velocity increases; persistence in either component appears as a growth in area as velocity increases. In the second study, 84 neurons were studied with proximal-to-distal scanning at 20, 40, and 80 mm s^{-1}.

The unexpected result of the second study was that scanning velocity had virtually no effect on the spatial structure of the neural responses or the estimated RFs. The RF structure was analyzed in three ways: (1) Area and mass. A fourfold increase in scanning velocity from 20 to 80 mm s^{-1} produced only a small increase in excitatory and inhibitory area (20% average growth in each) but the excitatory and inhibitory masses approximately doubled (86% and 144% increases in excitatory and inhibitory masses, respectively). The mean firing rate among these 84 neurons rose by 40% between 20 and 80 mm s^{-1}. This growth in area is consistent with excitation and inhibition that persist for about 10 ms. (2) Correlation. The most thorough analysis of similarity or dissimilarity in RF structure determined at different scanning velocities comes from a point-by-point correlation of pairs of RFs. Correlation coefficients between RFs estimated at different velocities ranged between 0.7

Fig. 1. A typical neural response and the resulting RF estimate. A. RF estimate. The gray scale represents the grid of weights (25×25 bins $= 10 \times 10$ mm) that best described the response of the neuron to the random dot stimulus pattern. The RF diagram is meant to represent excitatory and inhibitory skin regions viewed through the back of the finger as the finger points to the left and the stimulus pattern moves from right to left under the finger. The background gray level (50% black) represents the region where dots had no (linear) effect on the neural response, with darker levels representing excitatory regions where dots increased the probability of firing and lighter levels representing regions where dots decreased the probability of firing. B. A portion of the random dot stimulus pattern with the RF superimposed at three locations. The intensity of the RF gray scale has been reduced so the stimulus dots can be seen. C. Neural impulse rates predicted by convolving the RF (A) with the random dot stimulus (B) and by clipping negative values to zero. Darker regions correspond to higher predicted rates. The arrows extending from B to C point to the predicted impulse rates for each of the three RF positions in B. D. Observed response of this neuron. Each tick mark indicates the occurrence of a single spike. The plotted position of each spike was determined by the location of the stimulus pattern at the instant the spike occurred. The three vertical arrows indicate the responses at the stimulus locations corresponding to the three predicted responses in C. E. Predicted (black line) and observed (gray histogram) impulse rates in a single scan, whose location is indicated by the arrows at the sides of C and D. Predicted rates < 0 correspond to periods in which the summed inhibitory effects exceed the summed excitatory effects. From DiCarlo et al. [6]. Reprinted with permission.

and 1.0. Correlation is affected by both systematic changes in RF structure and noise in the RF estimates. The correlation coefficients between RFs estimated at 20 and 40 mm s^{-1} were, on average (mean $\Delta = 0.85$), only 0.03 correlation units lower than those expected from noise alone but the difference was significant ($P < 0.01$); the difference was 0.01 units for 40 and 80 mm s^{-1} (not significant) and 0.06 units for 20 and 80 mm s^{-1} ($P < 0.01$). (3) Centers of excitation and inhibition. A different analysis of spatial structure comes from identifying the centers of excitatory and inhibitory mass. The estimated center of excitatory mass moved distally by 0.20 mm between 20 and 40 mm s^{-1} and then a further 0.71 mm between 40 and 80 mm s^{-1}; thus, we can infer that the delay between the stimulus and the midpoint of the excitatory effect was 15 ms on average. The estimated center of inhibitory mass was, on average, distal to the center of excitation as in the first study and its estimated location moved distally with increasing velocity as expected. The surprising result was that its estimated location moved distally by only 0.19 mm between 20 and 40 mm s^{-1} and then a further 0.52 mm between 40 and 80 mm s^{-1}; that is, the estimated center of inhibition moved slightly closer to the excitation as the velocity increased. The principal point of these three analyses is that RF spatial structure is virtually unaffected by scanning velocity.

4. Study 3: random dots scanned in 4–8 directions at 40 mm s^{-1}

The evidence from the second study, taken alone, would suggest that there is no relative delay between the excitation and the inhibition—or even that inhibition leads excitation by a millisecond or two. The first and second studies taken together suggest that inhibition is, on average, displaced distally relative to excitation and that the two are synchronous. However, there is strong evidence from other studies that at least some of the inhibition lags behind the excitation by a substantial time period [1,10,14,22,35]. These competing possibilities can be tested by changing the scanning direction. If the excitation and inhibition occur simultaneously, or nearly so, then their relative positions will be unaffected by scanning direction. Conversely, if the inhibition is delayed substantially relative to excitation then its estimated position will tend to lag behind the excitation in the scanning direction whatever that direction may be. In fact, both effects were observed.

Sixty-two neurons provided reliable RF estimates in multiple directions (range 3–8, mean 5.1 directions; [8]). With a few exceptions discussed below, scanning direction had no discernible effect or only a small effect on firing rate. RFs estimated from responses to different scanning directions differed significantly from one another but in a systematic way. The central excitatory region was essentially unaffected by scanning direction; the RF differences between scanning directions were in the patterns of inhibition. Upon inspection it became evident that the inhibition comprised one (sometimes two) region whose position on the skin was unaffected by scanning direction and another region whose position depended on the scanning direction—generally trailing behind the excitation in the scanning direction. These observations suggested that each RF consisted of: (1) a central region of brief excitation, (2) a region of inhibition synchronous with the excitation, which we call fixed inhibition, and (3) a region of inhibition that lags behind the first two components. To test this hypothesis we constructed the RF model displayed in Fig. 2. Each RF was modeled with three Gaussian functions representing the three RF components. Each component was allowed to vary in intensity, spatial location, elongation, and orientation. The two inhibitory components were allowed to overlap the excitation, just as inhibition and excitation are known to overlap in the RFs of area 3b neurons [11,22]. The center of the

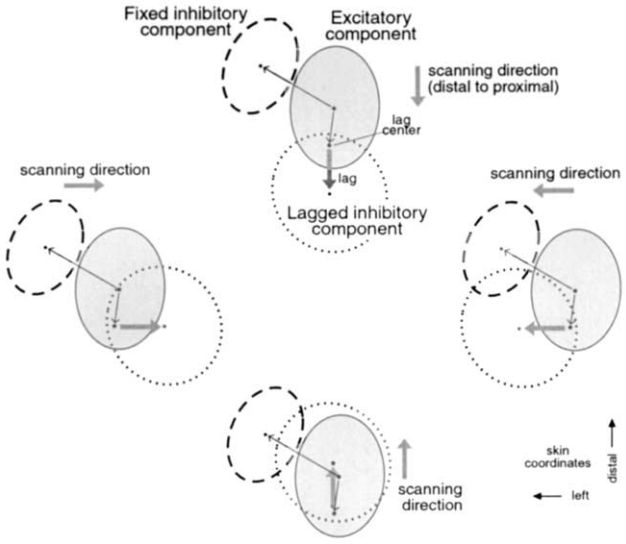

Fig. 2. Three-component Gaussian model. Three ellipses in each panel represent isoamplitude contours (at 1.5 SD) around Gaussian functions describing three RF components (excitatory, fixed inhibitory, and lagged inhibitory). The RF predicted by the model in each scanning direction (i.e. each panel) is the sum of these three Gaussian functions. Only the lagged inhibitory component changes its apparent RF location as scanning direction changes. This change in apparent RF location is the expected change if the lagged inhibitory component is temporally-delayed from the excitatory and fixed inhibitory components. The locations of the fixed inhibitory center and the lag center in relation to the excitatory subfield are identified by the two, thin arrows originating from the center of the excitatory component. The displacement of the lagged inhibitory component from the lag center is indicated by the thick, gray arrow. The tail of the gray arrow is at the lag center; the arrow direction corresponds to the stimulus direction across the RF (i.e. scanning direction). The tip of the gray arrow specifies the apparent location of the lagged inhibitory center. From DiCarlo and Johnson [8]. Reprinted with permission.

lagged inhibition trailed (in the scanning direction) behind a center at a fixed skin location, which we refer to as the lag center (Fig. 2). The lag center was not forced to coincide with the center of excitation. This three-component model described the RFs exceptionally well. The mean correlation between the model and the observed RFs was 0.81. A typical example of the fit between the model and the RFs for each direction is illustrated in Fig. 3. The only evident lack of fit was that some RFs had two regions of fixed inhibition rather than one. This could easily have been rectified by adding a second region of fixed inhibition to the model, which would have increased the correlation for several neurons substantially.

The excitatory and fixed inhibitory areas estimated by the model (Fig. 2) had nearly identical distributions and means (13.1 and 13.4 mm^2, respectively). The excitation was approximately four times more intense than the estimated fixed inhibition (means were 2440 and 571 mass units, respectively). The excitatory areas and intensities estimated by the model are slightly larger than those reported in the first study, as expected: when the net excitation and inhibition are calculated (i.e. the overlapping excitation and inhibition are canceled), they match the results of the first study closely. The centers of fixed inhibition were on average 2.5 mm from the center of excitation (Fig. 4; range 0.8–5.3 mm). The lagged inhibitory area and mass estimates averaged 24.0 mm^2 and 1781 mass units, respectively; the estimated lag averaged 29 ms (range 17–46 ms). This estimate is consistent with previous direct observations of the delay of inhibition relative to excitation [11,22] and of hyperpolarization relative to depolarization [1,14,35]. Because the lagged inhibitory RF component always

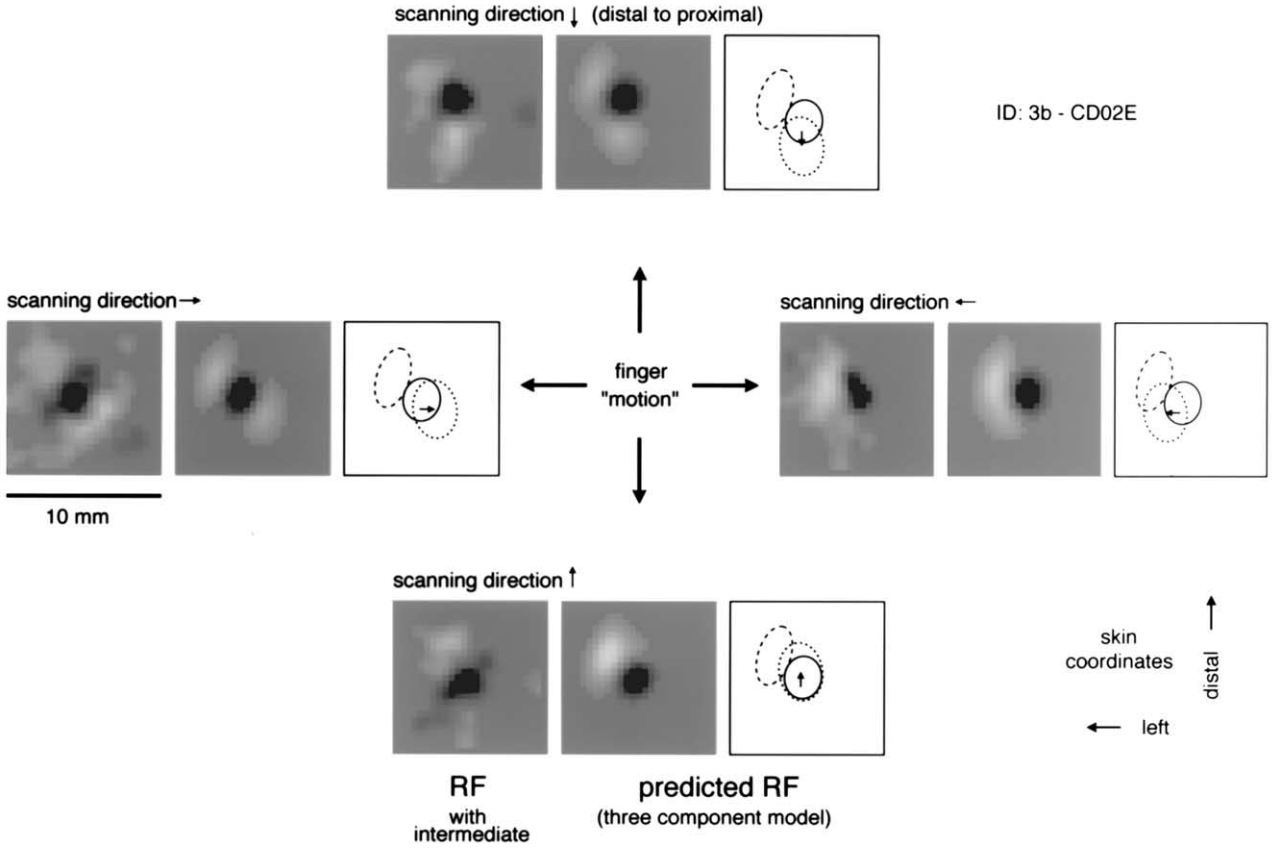

Fig. 3. RFs from a single area 3b neuron determined in four scanning directions and model predictions. The three squares in each group display the RF estimated from the raw data (on the left), the RF predicted by the three-component model (middle), and the positions of the model Gaussian components (on the right). The ellipses in the right square in each group are iso-amplitude contours at 1.5 SD as in Fig. 2. The scanning direction is shown above each group. Each RF is plotted as if it were viewed through the dorsum of the finger (i.e. from the neuron's point of view) with the finger pointed toward the top of the figure; the effect of relative motion between the finger and the stimulus pattern on the RF can be visualized by placing a fingerpad in the center of the figure and sliding it along the arrow labeled 'finger motion' toward the RF of interest. Note how the locations of the model's excitatory (solid ellipse) and fixed inhibitory components (dashed ellipse) are unaffected by scanning direction and, similarly, how the lagged inhibitory component (dotted ellipse) trails the lag center by a fixed distance in each direction (the distance is fixed because the scanning velocity is assumed to be constant; see Fig. 2). The arrow in each right-hand square corresponds to the gray arrow in Fig. 2. The degree to which the model accounts for RF structure in each direction can be seen by comparing the left and middle panels in each group. From DiCarlo and Johnson [8]. Reprinted with permission.

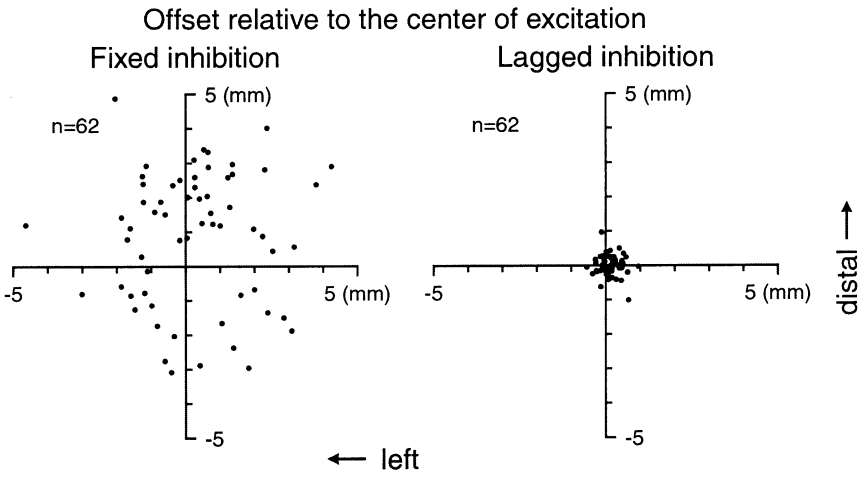

Fig. 4. Inhibitory offsets from the center of excitation. The left graph displays the locations of the centers of the fixed inhibitory components in relation to the centers of the excitatory components for all 62 neurons. The right graph displays the locations of the lag centers of the lagged inhibitory components in relation to the centers of the excitatory components. The data in both plots are displayed with the abscissa aligned from left to right. No obvious lateral bias is apparent when the data are plotted in these coordinates or in radial-ulnar coordinates. From DiCarlo and Johnson [8]. Reprinted with permission.

appears to trail the RF excitation in the scanning direction, it explains much of the distal bias in RF inhibition found in the first study.

Although the three-component model fits the data from the first and third study well, the presence of the lagged inhibitory RF component seems to contradict the second study. If a major component of the inhibition is delayed relative to the excitation, why is its apparent position unaffected by scanning velocity? Fig. 5 illustrates how RF structure can be invariant with changes in velocity even when the inhibition is delayed relative to excitation. The key point illustrated in Fig. 5 is that when the excitatory and inhibitory widths are larger than the displacement due to temporal delay between the two, the overall RF spatial structure is unchanged by changes in scanning velocity, but the excitatory and inhibitory intensities are affected strongly. However, the inhibition will always appear to lag the excitation in the scanning direction just as we observed in the third study.

The top two rows of Fig. 5 contain a simplified RF model that illustrates the key points. The model consists of uniform, rectangular regions of excitation and inhibition, 4.5 mm wide, that overlap in space but not in time: both the excitatory and inhibitory effects arise from the same skin region, but the inhibitory effect arrives 20 ms after the excitatory effect. When mapped with a scanned stimulus, this model matches qualitatively the RF features described in the second study [7]: (1) Inhibition appears to trail excitation in the scanning direction because its temporal delay appears as a spatial offset in the scanning direction. (2) Excitatory and inhibitory areas grow with increasing scanning velocity because the increasing, apparent displacement between excitation and inhibition with increasing velocity reduces the cancellation between them. (3) Net excitatory and inhibitory intensities (masses) increase with increasing scanning velocity for the same reason. (4) The distance between the apparent centers of excitation and inhibition is fixed and independent of scanning velocity because it is determined by the widths of the overlapping excitation and inhibition, not by the temporal delay. The bottom two rows of Fig. 5 are like the top two rows except that the excitatory and inhibitory effects are replaced with Gaussian functions. This produces results very similar to those reported in the second study. Net excitatory and inhibitory intensities (masses) increase much more with increasing velocity than do the excitatory and inhibitory areas. When the centers of excitation and inhibition and their displacements in the scanning direction are measured exactly the same way as in our study, the relative displacement between the apparent centers is unchanged even though the relative displacement between the actual centers of the overlapped excitation and inhibition change substantially.

In summary, the three-component model (Fig. 2) is capable of describing the RF results of all three of our studies and is consistent with data from previous studies [1,4,14,22]. The remainder of this manuscript is devoted to a discussion of the quality of the RF estimates and to the functional implications of three-component RF model.

5. Repeatability, goodness-of-fit, and generality

The quality of RF estimates of the kind we have presented here are indicated by three factors: repeatability, goodness-of-fit, and generality. Repeatability was assessed by subdividing the neural responses evoked

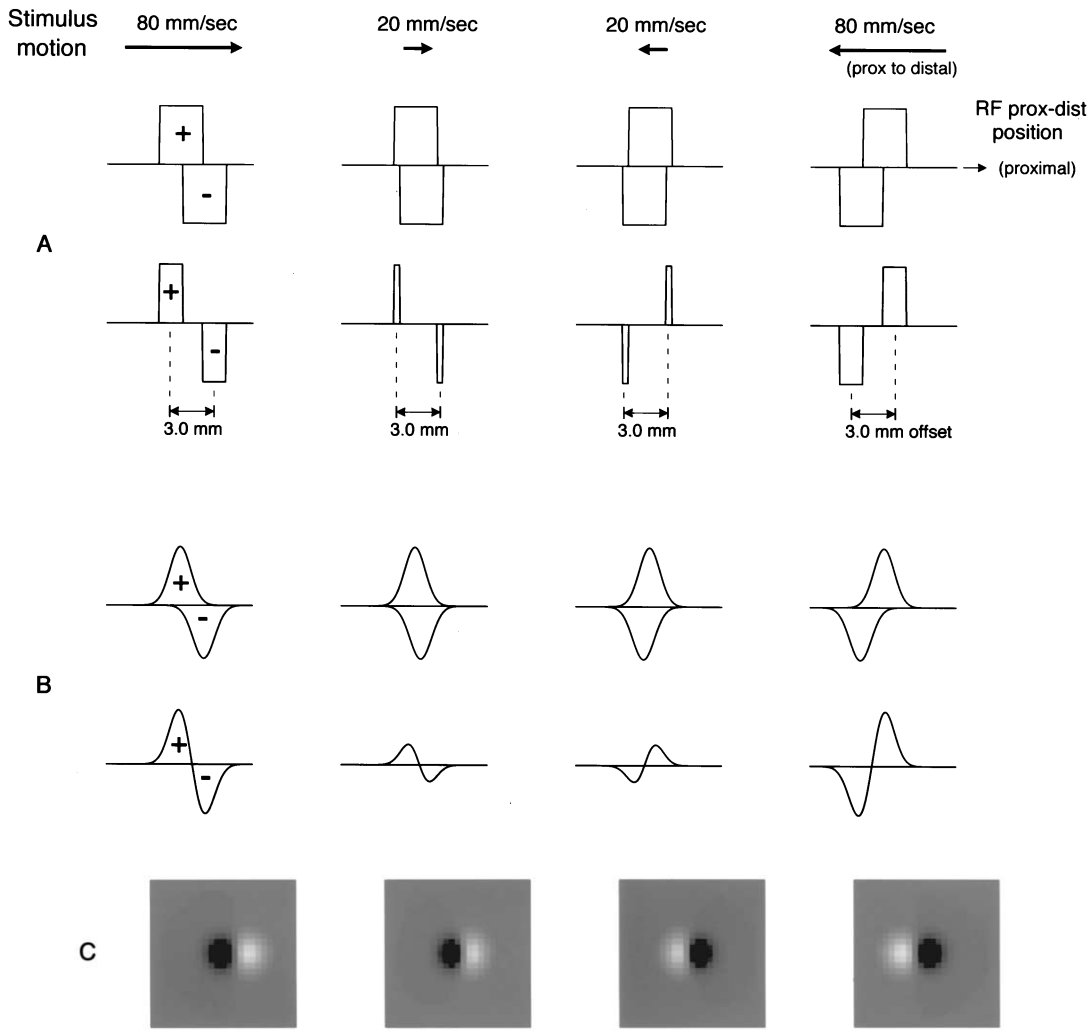

Fig. 5. One- and two-dimensional models illustrating possible effects of scanning velocity on RF geometry. These models illustrate how overlapping excitation and inhibition can produce increasing excitation and inhibition with increasing velocity with little change in RF spatial structure. The models assume inhibition that is spatially coextensive with excitation but is delayed 20 ms relative to the excitation. Profiles above (below) the line in each panel represent profiles of excitation (inhibition). The horizontal axis in each panel represents the location on the skin surface where the excitation or inhibition appears to have arisen. When the stimulus moves at a constant velocity and there is an unknown delay between the stimulus event on the skin and the effect on the neuronal discharge then the effect appears to have arisen from a location that is displaced from the true location by an amount proportional to the delay and the scanning velocity. When inhibitory delay is 20 ms greater than the excitatory delay, the skin region giving rise to inhibition appears to be displaced by 0.02*velocity (mm) relative to the apparent location of the excitation (the effect is 0.4 mm at 20 mm s^{-1}, 1.6 mm at 80 mm s^{-1}). A. The top row illustrates this effect at scanning velocities of 20 and 80 mm s^{-1} in both the proximal and distal directions. The second row illustrates the net effect (i.e. the observed RF) after accounting for the canceling effects of overlapping excitation and inhibition (assumed to be additive). Rectangular profiles, 3 mm wide, are illustrated for simplicity. Note how the offset between the observed centers of excitation and inhibition is unaffected by increases in scanning velocity and how the observed excitatory and inhibitory volumes (masses) increase. B. Gaussian excitatory and inhibitory profiles are meant to simulate more closely the RF profiles observed in this study. The inhibitory peak value is 10% less than the excitatory peak value, but its width is increased relative to the excitatory width so that they have equal mass. As in the simpler case illustrated above, the relative displacement between observed excitation and inhibition is affected little by changes in scanning velocity and both excitation and inhibition become more intense with increasing velocity. C. Gray scale plots of the RFs that would be observed in B. The correlation of the RFs illustrated at 20 and 80 mm s^{-1} is 0.95. From DiCarlo and Johnson [7]. Reprinted with permission.

by the scanned random-dot patterns in three different ways (alternating sweeps, first and last half of each drum revolution, and first and last 50 drum revolutions; [6]). Each method yielded two RF estimates. The repeatability between RF estimates was assessed by computing the correlation between RF estimates on a point-by-point basis (i.e. between the 625 RF bin values in each estimate). The paired RFs obtained by each method of subdividing the data were very similar. The correlation between RFs obtained from interleaved samples, which shows the lack of repeatability due to noise alone, averaged 0.89; the correlations between RFs based on the first and last half of each sweep, which includes effects of short term adaptation, averaged 0.85; the

correlation between the RFs obtained from the first and last 50 sweeps, which are data separated by 5–7 min of stimulation, averaged 0.81.

Goodness-of-fit for the RF estimates was assessed by computing the fraction of the explainable variance in the neural response that was accounted for by the RF estimate (i.e. the neural response predicted by the estimated RF; [6]). The observed discharge rate at any instant is the driven rate plus variability inherent in the spiking of cortical neurons. The RF estimate can predict the driven rate but not the stochastic component due to spiking. The explainable variance—the component that a good model can reasonably be assumed to account for—can be obtained by subtracting the stochastic variance from the total response variance; the stochastic variance can be estimated accurately by repeated measures in the same way that the intrinsic variance is separated from the response variance in an analysis of variance. On average, the responses predicted by the estimated RFs accounted for 40% of the explainable variance (which corresponds to a correlation coefficient of 0.63 between predicted and observed rates). The lack-of-fit is a reflection of the inability of the linear RF estimates to predict nonlinear response properties. To put this in perspective, we also studied the responses of SA1 and RA primary afferents with the same random-dot stimuli and estimated RFs in the same way. The linear RFs were able to account for only about 60% of the response variance (61% and 57% for SA1 and RA afferents, respectively) because of nonlinearities in the peripheral responses to complex spatial stimuli [26]. Because these nonlinearities are part of the neural responses of cortical neurons, any linear model can explain about 60% of the cortical response at most. The fact that the goodness-of-fit for many cortical responses is as high or nearly as high as for primary afferent responses suggests that the central mechanisms leading to their responses are approximately linear. However, for 100 of the 247 neurons analyzed in this way the linear RF accounted for less than 40% of the explainable variance. This suggests that a substantial part the lack of fit was due to central nonlinearities in many neurons.

Generality was assessed by comparing neural responses to oriented bars with the responses predicted by the three-component model derived from responses to random dot patterns. Of the 62 neurons that provided reliable RF estimates in multiple directions, 24 were studied with raised bars scanned in eight directions. The orientation sensitivity and preferred orientation were obtained by fitting an ellipse to the responses plotted on a polar plot (Fig. 6). The sensitivity (ratio of major to minor axis) ranged from 1.05 to 4.6 and 9/24 neurons had sensitivities >2. The predicted sensitivities and

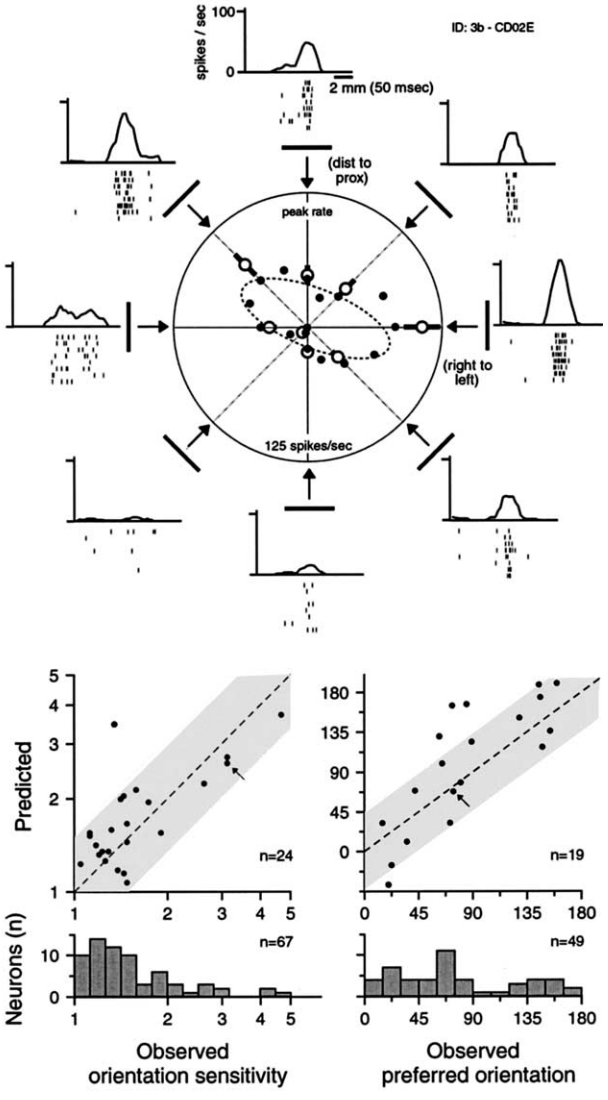

Fig. 6

Fig. 6. The top panel illustrates the responses of one of the more orientation-selective neurons that was also studied with the random-dot patterns. Each raster plot shows spikes (tick marks) produced in response to eight repeated scans of a single, raised bar scanned in a particular direction across the neuron's RF. The histogram above each raster shows the spike data binned across trials. The peak value of each histogram was taken as the neuron's response in that scanning direction and these values are plotted as open circles along the radial lines in the central polar plot. The 16 filled circles show the responses predicted by the three-component model for this neuron in 16 directions. The dashed line shows the ellipse that best fits the 16 predicted response values (least-squared radial error). The middle, left scatter plot shows the observed orientation sensitivity (ellipse aspect ratio) on the abscissa and the predicted orientation sensitivity on the ordinate for 24 neurons whose three-component RF models and orientation sensitivities were determined. The right scatter plot shows the observed preferred orientation (ellipse angle) on the abscissa and the predicted preferred orientation on the ordinate for 19 of these 24 neurons whose observed orientation sensitivities were greater than 1.2. The small arrow in each scatter plot indicates the datum from the neuron illustrated in the top panel. The bottom two panels show the distributions of observed orientation sensitivities and observed preferred orientations (for neurons with orientation sensitivities greater than 1.2). From DiCarlo and Johnson [8]. Reprinted with permission.

orientations matched the observed values closely ($\Delta =$ 0.71 and 0.81 for sensitivity and orientation. respectively).

6. Relationship to cortical layer

The mean values of orientation sensitivity and the ratio of fixed inhibitory mass to excitatory mass in layer III were almost twice as great as in the other layers (Fig. 7). Twelve of 40 neurons whose laminar locations were identified had orientation selectivities >1.5, and all but one of those were in the infragranular or supragranular layers. There are strong excitatory projections from granular to supragranular layers [31] and projections to higher cortical areas (e.g. SII) arise mainly from the supragranular layers [19]. Physiological studies reveal larger RF sizes [32] and more complex spatial response properties [5] in supragranular (vs. granular) layers. Thus, it appears that selectivity for spatial form increases within area 3b before the neural representation of a tactile stimulus is relayed to higher cortical areas.

7. Functional implications

The fixed excitatory and inhibitory components of each neuron function as a spatial filter, conferring selectivity for particular spatial features or patterns regardless of scanning direction and velocity. Raster plots of the responses of area 3b neuron to scanned, complex patterns like raised letters show that many neurons are selective for the features of complex stimuli [2,6,27] and that these responses are explained in whole or in part by linear RFs [6,18]. Also, neurons in area 3b are moderately orientation selective [13,29,34]. We confirmed this observation and showed that this orientation sensitivity is predicted by the three-component RF model (Fig. 2). The RF property most strongly associated with orientation sensitivity was the ratio of fixed inhibitory to excitatory mass.

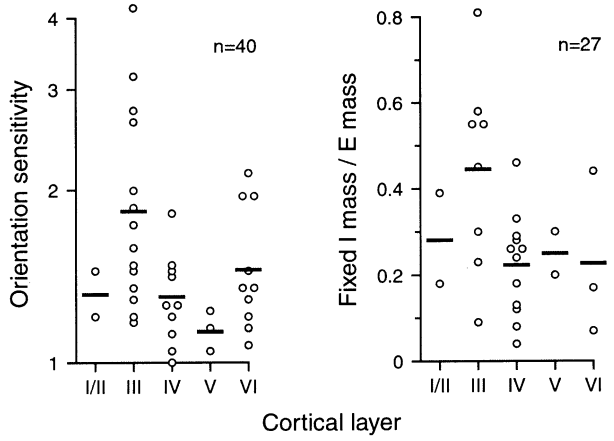

Fig. 7. Relationship of orientation sensitivity and RF mass ratio to cortical layer. The abscissa of both plots is the cortical layer in which each neuron was recorded. The ordinate of the left plot is the observed orientation sensitivity. Forty area 3b neurons whose cortical layer and orientation sensitivity were determined are shown. The ordinate of the right plot is the ratio of the mass of the fixed inhibitory RF component and the mass of the excitatory RF component. Twenty-seven area 3b neurons whose cortical layer and three-component RF models were both determined are shown. The thick bars in each plot indicate the mean value in each cortical layer. From DiCarlo and Johnson [8]. Reprinted with permission.

The lagged inhibitory component confers sensitivity for stimulus gradients and features in the scanning direction, regardless of that direction. When scanning the finger over a uniform surface, elevations trigger the excitation first and then the lagged inhibition 30 ms later. This suppresses the response to uniform surfaces and thereby emphasizes the effects of spatial or temporal novelty. In addition, if the lag center is substantially displaced from the center of excitation, directional selectivity is expected. When the stimulus is scanned in a direction defined by a vector from the center of excitation to the lag center (Fig. 2), the lagged inhibition is displaced away from the excitation and uncovers it maximally; this should maximize the firing rate. In the opposite direction the lagged inhibition swings over the excitation and masks it maximally; this should minimize the firing rate [3,12,34]. The lag offsets were generally small in our study (mean 0.35 mm), which minimizes this effect, but three neurons had offsets close to 1 mm (Fig. 4). These three neurons also had higher response rates for the scanning direction predicted by the lag offset. The generally small lag offsets (Fig. 4) and mild directional selectivities observed in the present study are consistent with previous reports of substantial directional selectivity in only a few neurons [4,30,34].

Perhaps a more important role played by overlapping, lagged inhibition is to compensate for changes in scanning velocity. The acquisition of tactile spatial information by scanning movements compensates for the very limited field of view provided by a single fingerpad. It is clearly an advantage to be able to scan one's fingers over an object or a surface rapidly without loss of spatial acuity. However, rapid scanning has a cost. As scanning velocity increases, each stimulus element spends less time within the RF (reduced dwell time) and the element is represented by fewer action potentials unless some mechanism increases the neuron's sensitivity. Other factors such as differences in latency between different response components, persistence of excitatory and inhibitory effects, and conduction velocity dispersion in the afferent pathways [16] tend to degrade the spatial integrity of a moving neural image. Nonetheless, psychophysical experiments demonstrate little loss of spatial acuity at scanning rates up to at least 80 mm s^{-1} [33]. This, in turn, implies that mechanisms at all levels within the pathways leading to perception

maintain the integrity of spatial information over this range of scanning velocities. Primary afferent fibers, which are much more sensitive to dynamic than stationary stimuli, compensate for increased scanning velocities with increasing firing rates [9,16,21,28]. Cortical neurons compensate by the lagged inhibition, which lags progressively to expose more excitation as the scanning velocity increases. The mechanisms that we have suggested in Fig. 5 serve to maintain structural invariance even as the progressive lag produces increasing excitation. Whether this suggested mechanism is correct or not, the data from these studies demonstrate that area 3b responses are essentially invariant over a wide range of scanning velocities. This invariance is consistent with the hypothesis that area 3b plays a critical role in tactile spatial perception including roughness estimation and form recognition, which are also unaffected by changes in scanning velocity [20,23,24,33].

Acknowledgements

The research reported here was supported by NIH grant NS18787.

References

[1] Andersson SA. Intracellular postsynaptic potentials in the somatosensory cortex of the cat. Nature 1965;205:297–8.
[2] Bankman IN, Johnson KO, Hsiao SS. Neural image transformation in the somatosensory system of the monkey: Comparison of neurophysiological observations with responses in a neural network model. Cold Spring Harb Symp: Quant Biol 1990;55:611–20.
[3] Barlow HB, Levick WR. The mechanism of directionally selective units in rabbit's retina. J Physiol London 1965;178:477–504.
[4] Costanzo RM, Gardner EP. A quantitative analysis of responses of direction-sensitive neurons in somatosensory cortex of awake monkeys. J Neurophysiol 1980;43:1319–41.
[5] DiCarlo JJ, Hsiao SS, Johnson KO. Transformation of tactile spatial form within a cortical column in area 3b of the macaque. Soc Neurosci Abstr 1994;20:1387.
[6] DiCarlo JJ, Johnson KO, Hsiao SS. Structure of receptive fields in area 3b of primary somatosensory cortex in the alert monkey. J Neurosci 1998;18:2626–45.
[7] DiCarlo JJ, Johnson KO. Velocity invariance of receptive field structure in somatosensory cortical area 3b of the alert monkey. J Neurosci 1999;19:401–19.
[8] DiCarlo JJ, Johnson KO. Spatial and temporal structure of receptive fields in primate somatosensory area 3b: effects of stimulus scanning direction and orientation. J Neurosci 2000;20:495–510.
[9] Essick GK, Edin BB. Receptor encoding of moving tactile stimuli in humans. II. The mean response of individual low-threshold mechanoreceptors to motion across the receptive field. J Neurosci 1995;15:848–64.
[10] Gardner EP, Costanzo RM. Temporal integration of multiple-point stimuli in primary somatosensory cortical receptive fields of alert monkeys. J Neurophysiol 1980;43:444–68.
[11] Gardner EP, Costanzo RM. Spatial integration of multiple-point stimuli in primary somatosensory cortical receptive fields of alert monkeys. J Neurophysiol 1980;43:420–43.
[12] Gardner EP, Costanzo RM. Neuronal mechanisms underlying direction sensitivity of somatosensory cortical neurons in awake monkeys. J Neurophysiol 1980;43:1342–54.
[13] Hyvärinen J, Poranen A. Movement-sensitive and direction and orientation-selective cutaneous receptive fields in the hand area of the post-central gyrus in monkeys. J Physiol London 1978;283:523–37.
[14] Innocenti GM, Manzoni T. Response patterns of somatosensory cortical neurones to peripheral stimuli. An intracellular study. Arch Ital Biol 1972;110:322–47.
[15] Iwamura Y, Tanaka M, Sakamoto M, Hikosaka O. Functional subdivisions representing different finger regions in area 3 of the first somatosensory cortex of the conscious monkey. Exp Brain Res 1983;51:315–26.
[16] Johnson KO, Lamb GD. Neural mechanisms of spatial tactile discrimination: neural patterns evoked by Braille-like dot patterns in the monkey. J Physiol London 1981;310:117–44.
[17] Johnson KO, Phillips JR. A rotating drum stimulator for scanning embossed patterns and textures across the skin. J Neurosci Methods 1988;22:221–31.
[18] Johnson KO, Hsiao SS, Twombly IA. Neural mechanisms of tactile form recognition. In: Gazzaniga MS, editor. The cognitive neurosciences. Cambridge, MA: MIT Press, 1995:235–68.
[19] Jones EG. Laminar distribution of cortical efferent cells. In: Peters A, et al, editor. Cerebral cortex. Cellular components of the cerebral cortex, vol. 1. New York: Plenum, 1984:521–54.
[20] Katz D. The world of touch. In: Erlbaum, editor. NJ: Hillsdale; 1925. [Krueger LE, Trans.; original work published 1925.]
[21] Lamb GD. Tactile discrimination of textured surfaces: peripheral neural coding in the monkey. J Physiol London 1983;338:567–87.
[22] Laskin SE, Spencer WA. Cutaneous masking. II. Geometry of excitatory and inhibitory receptive fields of single units in somatosensory cortex of the cat. J Neurophysiol 1979;42:1061–82.
[23] Lederman SJ. Tactile roughness of grooved surfaces: The touching process and the effects of macro- and microsurface structure. Percept Psychophys 1974;16:385–95.
[24] Lederman SJ. Tactual roughness perception: Spatial and temporal determinants. Can J Psychol 1983;37:498–511.
[25] Mountcastle VB, Powell TPS. Neural mechanisms subserving cutaneous sensibility, with special reference to the role of afferent inhibition in sensory perception and discrimination. Bull Johns Hopkins Hosp 1959;105:201–32.
[26] Phillips JR, Johnson KO. Tactile spatial resolution: III. A continuum mechanics model of skin predicting mechanoreceptor responses to bars, edges, and gratings. J Neurophysiol 1981;46:1204–25.
[27] Phillips JR, Johnson KO, Hsiao SS. Spatial pattern representation and transformation in monkey somatosensory cortex. Proc Natl Acad Sci USA 1988;85:1317–21.
[28] Phillips JR, Johansson RS, Johnson KO. Responses of human mechanoreceptive afferents to embossed dot arrays scanned across fingerpad skin. J Neurosci 1992;12:827–39.
[29] Pubols BH, Jr, LeRoy RF. Orientation detectors in the primary somatosensory neocortex of the raccoon. Brain Res 1977;129:61–74.
[30] Ruiz S, Crespo P, Romo R. Representation of moving tactile stimuli in the somatic sensory cortex of awake monkeys. J Neurophysiol 1995;73:525–37.
[31] Schwark HD, Jones EG. The distribution of intrinsic cortical axons in area 3b of cat primary somatosensory cortex. Exp Brain Res 1989;78:501–13.

[32] Sur M, Garraghty PE, Bruce CJ. Somatosensory cortex in macaque monkeys: laminar differences in receptive field size in areas 3b and 1. Brain Res 1985;342:391–5.
[33] Vega-Bermudez F, Johnson KO, Hsiao SS. Human tactile pattern recognition: Active versus passive touch, velocity effects, and patterns of confusion. J Neurophysiol 1991;65:531–46.
[34] Warren S, Hämäläinen HA, Gardner EP. Objective classification of motion- and direction-sensitive neurons in primary somatosensory cortex of awake monkeys. J Neurophysiol 1986;56:598–622.
[35] Whitehorn D, Towe AL. Postsynaptic potential patterns evoked upon cells in sensorimotor cortex of cat by stimulation at the periphery. Exp Neurol 1968;22:222–42.
[36] Whitsel BL, Roppolo JR, Werner G. Cortical information processing of stimulus motion on primate skin. J Neurophysiol 1972;35:691–717.